Numerical Studies of the Cahn–Hilliard Equation for Phase Separation

CHARLES M. ELLIOTT

School of Mathematical and Physical Sciences, University of Sussex, Brighton BN1 9QH, England

AND

DONALD A. FRENCH

Department of Mathematics, Purdue University, West Lafayette, IN 47907 USA

Phase separation in a binary mixture is described by the nonlinear evolutionary Cahn–Hilliard equation. In this paper, we discuss the physical background of the equation and describe its solution by the Galerkin finite element method. Some theoretical results are presented and computationally verified.

1. Introduction

IN this paper we study the behaviour of the solution $u(x, t)$ of the nonlinear evolution equation

$$u_t + \gamma D^4 u = D^2 \phi(u) \quad (0 < x < L, 0 < t), \tag{1.1a}$$

where

$$\phi(u) = \gamma_2 u^3 + \gamma_1 u^2 + \gamma_0 u, \tag{1.1b}$$

subject to the boundary conditions

$$Du = \gamma D^3 u - D\phi(u) = 0 \quad (x = 0, x = L) \tag{1.1c}$$

and initial condition

$$u(x, 0) = u_0(x). \tag{1.1d}$$

Here $D \equiv \partial/\partial x$, γ is a prescribed positive constant, and γ_0, γ_1, and γ_2 are given constants. This initial-boundary-value problem arises in the study of phase separation in binary solutions; cf. Novick-Cohen & Segel (1984). In Section 2 of this paper, we motivate the study of (1.1) by describing its application to phase separation, and we discuss some mathematical results concerning $u(x, t)$. For other applications, we refer to Cohen & Murray (1981), Hazewinkel, Kasshoek, & Leynse (1985). See also Gurtin (1986) and Modica (1987).

The solution possesses interesting asymptotic behaviour and spatial structure. This is studied numerically in Section 4, using a finite element Galerkin method

described in Section 3. In Section 5, future research directions on this problem are discussed; in particular, the idea of metastability is addressed.

Throughout the paper, the norms of $L^\infty(I)$, $L^2(I)$, and $H^s(I)$ are denoted by $\|\cdot\|_\infty$, $\|\cdot\|_0$, and $\|\cdot\|_s$. The seminorm $\|D^s v\|_0$ is denoted by $|v|_s$.

2. Phase separation and the Cahn–Hilliard equation

Let $\mathcal{M}$ be a binary mixture composed of two species X_A and X_B. Below a critical temperature T_C, thermodynamic equilibrium corresponds to a coexistence of two phases, one phase rich in species X_B and the other phase rich in X_A. Let $u(x, t)$ denote the (appropriately scaled) concentration of species X_B. Associated with the mixture is a Ginzburg–Landau free energy $\Psi(u, T)$ which, for $T < T_C$, has the double-well form shown in Fig. 2.1.
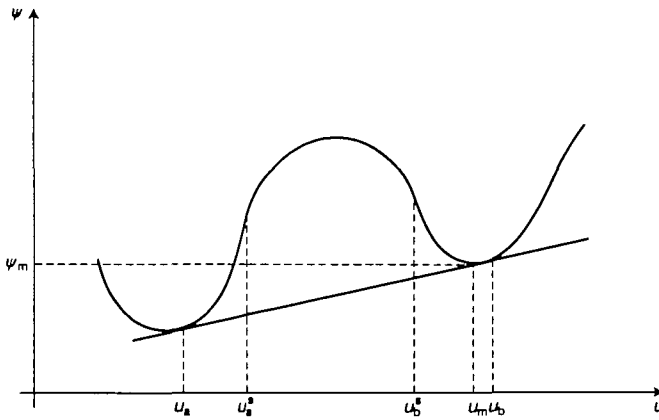

FIG. 2.1. Free energy.

The interval (u_a^s, u_b^s) is said to be the spinodal interval; u_a^s and u_b^s are spinodal points and are defined by the condition $\partial^2 \Psi/\partial u^2 < 0$ in (u_a^s, u_b^s) and $\partial^2 \Psi/\partial u^2 > 0$ outside the interval $[u_a^s, u_b^s]$. Close to the two local minima are the binodal values u_a and u_b, which are the two unique points where the supporting tangent touches the curve. We can show that these values define piecewise constant functions that minimize the free energy functional

$$F(v) = \int_I \Psi(v, T)\, dx \tag{2.1a}$$

over all concentration distributions satisfying the prescribed mass constraint

$$\int_I u\, dx = ML, \tag{2.1b}$$
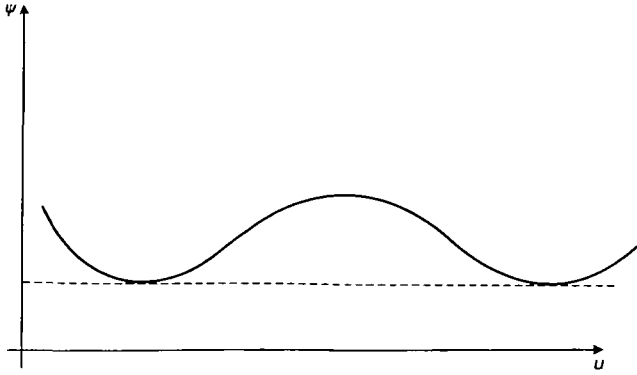
provided that

$$u_a < M < u_b. \tag{2.1c}$$

FIG. 2.2. Special case

This is clearly true if Ψ has the special shape in Fig. 2.2.

For general Ψ, let

$$\bar{\Psi}(v) = \Psi(v) - \alpha v$$

where α is a fixed constant. Note that

$$F(v) = \bar{F}(v) - \alpha M$$

if

$$\bar{F}(v) = \int_I \bar{\Psi}(v)\, dx.$$

For fixed α, minimizing F is equivalent to minimizing $\bar{F}$. Choosing α equal to the slope of the supporting tangent line makes $\bar{\Psi}$ have the same shape as the function in Fig. 2.2. Piecewise constant functions that satisfy (2.1b) with values at the minima of $\bar{\Psi}$ will minimize $F(v)$. These critical points are the binodal points described above; they are also determined by the conditions

$$\Psi'(u_a) = \Psi'(u_b) = \frac{\Psi(u_b) - \Psi(u_a)}{u_b - u_a} = \alpha.$$

The spinodal region is unstable, states to the left and right of the binodal points are stable, and the remaining intervals are metastable. Suppose that the mixture $\mathcal{M}$ has been prepared to have an initial state with a spatial composition taking values in the spinodal interval. The mixture will evolve from this unstable nonequilibrium state to an equilibrium configuration consisting of two coexisting phases with a spatial pattern composed of 'grains' rich in either X_A or X_B. Such an evolution process is called phase separation and, when it takes place in the spinodal region, it is called spinodal decomposition; see Cahn (1961), (1962), Langer (1971), Gunton, San-Miguel, & Sahni (1983), and Koch (1984). It then slowly loses some of these grains, tending toward more stable patterns; this process is called ripening or coarsening.

The first continuum model of this phenomenon is due to Cahn–Hilliard (1958),

who considered an isothermal system and proposed the generalized diffusion equation

$$u_t + DJ = 0, \qquad (2.2a)$$

where the mass flux J satisfies

$$J = -D(\Psi_u - \gamma D^2 u) = -D\sigma \qquad (2.2b)$$

and σ is a local chemical potential defined to be the functional derivative of the extended Ginzberg–Landau free-energy functional

$$\mathscr{F}(u) = \int_I \left(\Psi + \frac{\gamma}{2} |Du|^2 \right) dx. \qquad (2.3)$$

The second term in this integral is a phenomenological quantity representing the interfacial surface energy due to spatial inhomogeneities in the concentration. Equation (2.2) is supplemented by the boundary conditions

$$D(\Psi_u - \gamma D^2 u) = 0 \quad (x = 0, L), \qquad \gamma Du = 0 \quad (x = 0, L) \qquad (2.4a,b)$$

and initial condition

$$u(x, 0) = u_0(x), \qquad \int_I u_0(x) \, dx = ML. \qquad (2.5)$$

Equations (2.4b) are the natural boundary conditions for finding critical points of $\mathscr{F}(\cdot)$ and equations (2.4a) are zero mass flux conditions which imply that mass is conserved:

$$\int_I u(x, t) \, dx = \int_I u_0(x) \, dx = ML \quad (t > 0). \qquad (2.6)$$

The simplest form of Ψ having the double-well potential is

$$\Psi(u) = \tfrac{1}{4}\gamma_2 u^4 + \tfrac{1}{3}\gamma_1 u^3 + \tfrac{1}{2}\gamma_0 u^2, \qquad (2.7)$$

where $\gamma_2 > 0$ and the quadratic

$$\Psi''(u) = 3\gamma_2 u^2 + 2\gamma_1 u + \gamma_0 \qquad (2.8)$$

has two real roots: the spinodal values u_a^s and u_b^s. We identify

$$\phi(u) = \Psi'(u) \qquad (2.9)$$

so that (1.1a) is the Cahn–Hilliard equation (2.2), and assume that ϕ has three real roots with the property that Ψ is strictly convex at its two local minima.

The initial-boundary-value problem (1.1) was studied by Elliott & Zheng (1986) and Zheng (1986). The existence of a solution locally in time is proved by standard Picard iteration. Global existence results are obtained by proving a priori estimates for the appropriate norms of u. We introduce the notation

$$H_E^2(I) = \{ \eta \in H^2(I) : D\eta = 0 \ (x = 0, L) \}$$

and assume that $u_0 \in H_E^2(I)$.

THEOREM 2.1   *Under the above assumptions on $\phi(\cdot)$ and u_0:*

   (i) *There exists a unique solution to (1.1) for each $T > 0$ such that*

$$u \in L^2(0, T; H^4(I)), \qquad u_t \in L^2(0, T; L^2(I)).$$

   (ii) *If $u_0 \in H^6(I) \cap H_E^2(I)$ and $D^2 u_0 \in H_E^2(I)$, then the solution to (1.1) is a classical one.*

   (iii) *For any initial data, the solution $u(t)$ converges as $t \to \infty$ to a solution of the steady-state problem.*

$$\gamma D^2 u = \phi(u) - \sigma \quad (0 < x < L),$$

$$D u = 0 \quad (x = 0, L), \qquad \int_I u \, dx = ML \tag{2.10}$$

where $\sigma \in \mathbb{R}$ is to be determined.

   (iv) *The solution of problem (2.10) is equivalent to finding critical points of $\mathcal{F}(u)$ over the space of functions in $H^1(\Omega)$ whose mean value is M.*

   (v) *The solution will converge in $H_E^2(I)$ as $t \to \infty$ to the uniform state $u = M$, provided that any of the following conditions hold:*
   (C1) *$\gamma > L^2/\pi^2$ and $\|u_0\|_2$ is sufficiently small.*
   (C2) *$|M|$ is sufficiently large.*
   (C3)

$$\int_I [\Psi(u_0) - \Psi_m] \, dx + \frac{\gamma}{2} |u_0|_1^2$$

is sufficiently small, $\Psi(u_0) > \Psi_m$ for all x, Ψ_m is either of the local minima of $\Psi(s)$ on $\mathbb{R}$, and M is sufficiently close to u_m, where $\Psi_m = \Psi(u_m)$.

Proof. Results (i) and (ii) were proved by Elliott & Zheng (1986) with $\gamma_0 = -1$. However their proof remains the same for general γ_0. The result (iii) concerning the asymptotic behaviour of $u(t)$ as $t \to \infty$ was proved by Zheng (1986) using the idea of the ω-limit set. That (2.10) is the steady state of (1.1) follows from setting $u_t = 0$ and integrating with respect to x twice, using the zero mass flux condition. The constant steady-state chemical potential σ is determined by the prescribed mass condition. Result (iv) is Lemma 3.1 of Zheng (1986).

It is clear that $u = M$ is a solution of (2.10), and (v) lists sufficient conditions for the convergence of $u(t)$ to M as $t \to \infty$. The sufficiency of (C1) was proved by Elliott & Zheng (1986) and that of (C2) by Zheng (1986). Indeed, if M is sufficiently large, then (2.10) has the unique solution $u = M$.

To verify (C3) we use the useful fact that $\mathcal{F}(u)$ is a Lyapunov functional. A simple calculation reveals

$$\frac{d}{dt} \mathcal{F}(u) = \int_I \left(\phi(u) \frac{\partial u}{\partial t} + \gamma D u D \frac{\partial u}{\partial t} \right) dx$$

$$= - \int_I (\gamma D^3 u - D\phi)^2 \, dx.$$

It follows that, for all t,

$$\int_I \Psi(u)\, dx + \frac{\gamma}{2}|u|_1^2 \leq \int_I \Psi(u_0)\, dx + \frac{\gamma}{2}|u_0|_1^2 \qquad (2.11)$$

and, from the Sobolev imbedding theorem and the Poincaré inequality,

$$\int_I \Psi(u)\, dx + \frac{c\gamma}{2}\|u - M\|_\infty \leq \int_I \Psi(u_0)\, dx + \frac{\gamma}{2}|u|_1^2.$$

Using the triangle inequality, this becomes

$$\int_I [\Psi(u) - \Psi_m]\, dx + \frac{c\gamma}{2}\|u - u_m\|_\infty$$
$$\leq \int_I [\Psi(u_0) - \Psi_m]\, dx + \frac{c\gamma}{2}|u_m - M| + \frac{\gamma}{2}|u|_1^2 = \varepsilon, \quad (2.12)$$

where u_m is a local minimum of Ψ and $\Psi_m = \Psi(u_m)$. (See Fig. 2.1.)

We can make ε as small as we like by requiring M to be close to u_m and the first derivative of u_0 is small. If we take u_0 so that

$$\varepsilon < \tfrac{1}{4}c\gamma(u_m - u_b^s), \qquad \int_I [\Psi(u_0) - \Psi_m]\, dx \geq 0,$$

then, from (2.12), we claim that

$$\|u(\cdot, t) - u_m\|_\infty < u_m - u_b^s. \qquad (2.13)$$

for all t.

To see this, note that $\|u_0 - u_m\|_\infty < u_m - u_b^s$, so (2.13) holds by continuity at least for a short time. Suppose the inequality is first violated at $t^* > 0$:

$$\|u(\cdot, t^*) - u_m\|_\infty \geq u_m - u_b^s. \qquad (2.14)$$

On $[0, t^*)$, we have

$$\int_I [\Psi(u(\cdot, t)) - \Psi_m]\, dx \geq 0,$$

so $\tfrac{1}{2}c\gamma\|u(\cdot, t) - u_m\|_\infty \leq \varepsilon < \tfrac{1}{4}c\gamma(u_m - u_b^s)$, i.e.

$$\|u(\cdot, t) - u_m\|_\infty < \tfrac{1}{2}(u_m - u_b^s),$$

which contradicts (2.14).

Condition (2.13) implies $\Psi''(u) \geq 0$ for all t. Multiplying equation (1.1a) by $u - M$ and integrating with respect to x yields

$$\tfrac{1}{2}\frac{d}{dt}\|u - M\|_0^2 + \gamma |u|_2^2 \leq -(\Psi''(u)u_x, u_x) \leq 0,$$

where $(\cdot, \cdot)$ is the standard $L^2(I)$ inner product. Since $\|u - M\|_0 \leq c |u|_2$, Gronwall's inequality gives $\|u - M\|_0 \leq e^{-\alpha}\|u_0 - M\|_0$, which proves (C3) □

Remarks. (1) The steady-state problem is equivalent to finding the critical points

of the functional $\mathcal{F}(v)$ over $\{H^1(I) : Dv = 0 \ (x = 0, L), \int_I v \, dx = ML\}$. However, when $\gamma = 0$, we have the problem (2.1) which has a continuum of solutions consisting of piecewise constant distributions with the constants being either u_a or u_b, and with the prescribed mass conditions (2.1b) holding. It follows that we may expect, for small γ, steady-state solutions with an oscillating structure. See also Elliott (1985) for the numerical solutions of a related evolutionary problem with $\gamma = 0$.

(2) The behaviour of solutions to (2.10) was analysed in Carr, Gurtin & Slemrod (1984). They showed that

(i) If γ is sufficiently small, then $\mathcal{F}(u)$ has a unique minimum function u_γ, which is monotone (its *reversal* $u_\gamma(-x)$ has the same free energy);

(ii) all nonmonotone solutions of the steady state problem (2.10) are saddle points of $\mathcal{F}(u)$;

(iii) steady solutions are periodic in the sense that all lengths along the x-axis of transitions, from peak to trough or vice versa, are equal.

Statement (ii) guarantees that, at any nonmonotone solution $\bar{u}$ of (2.10), there is a direction v so, for α_0 sufficiently small, we have

$$\mathcal{F}(\bar{u} + \alpha v) < \mathcal{F}(\bar{u}) \quad (0 < \alpha \leqslant \alpha_0).$$

Since $\mathcal{F}$ is a Lyapunov functional there is initial data u_0 lying in any H^1 neighbourhood of $\bar{u}$ for which the solution of the dynamic problem (1.1) will stay bounded away from $\bar{u}$.

(3) Zheng (1986) has shown (See also Carr, Gurtin & Slemrod (1984)) that, if

$$\phi(u) = u^3 - u, \qquad M = 0, \qquad N_0 \leqslant 4/\pi L \gamma^{\frac{1}{2}} < N_0 + 1,$$

then the steady-state problem has exactly $2N_0 + 1$ solutions. We note that one solution is $u = 0$ and that, if $u(x)$ is a solution, then $-u(x)$ is also a solution.

(4) Under conditions (C1), (C2), and (C3), phase separation does not take place.

(5) If we consider (1.1) with $\gamma_2 < 0$, then Elliott & Zheng (1986) have proved that, if $-\mathcal{F}(u_0)$ is sufficiently large, then there exists a $T^* > 0$ such that

$$\|u(\cdot, t)\|_2 \to \infty \quad \text{as } t \to T^*$$

i.e. the solution blows up in finite time.

3. Numerical method

Let S_h^r be the piecewise polynomial spline space

$$S_h^r = \{\chi \in C^{r-2}(I) : \chi \upharpoonright I_j \in P_{r-1}(I_j) \ (j = 1, \ldots, J)\},$$

where $r \geqslant 3$ is an integer,

$$0 = x_0 < x_1 < \cdots < x_J = L$$

is a partition of $I = (0, L)$ with $I_j = (x_{j-1}, x_j)$, and $P_{r-1}(I_j)$ denotes the set of all

polynomial functions on I_j of degree less than or equal to $r - 1$. Define

$$\mathring{S}_h^r = \{\chi \in S_h^r : D\chi(0) = D\chi(L) = 0\}, \qquad h = \max_{1 \leq j \leq J} (x_j - x_{j-1}),$$

and let

$$\alpha \geq h \left(\min_{1 \leq j \leq J} (x_j - x_{j-1}) \right)^{-1},$$

where we assume that, for a family of partitions, α is fixed.

The approximation scheme using a Galerkin method in space and an implicit midpoint time discretization is: find $\{U^n\}_{n=1}^{N}$ such that $U^n \in \mathring{S}_h^r$ and

$$(\partial_t U^n, \chi) + \gamma(D^2 U^{n+\frac{1}{2}}, D^2\chi) = (\phi(U^{n+\frac{1}{2}}), D^2\chi) \quad \forall \chi \in \mathring{S}_h^r \qquad (3.1a)$$

with

$$U^0 = u_0^h, \qquad (3.1b)$$

where u_0^h is an appropriate approximation to u_0. In (3.1) we have used the notation

$$\partial_t V^n = k^{-1}(V^{n+1} - V^n), \qquad V^{n+\frac{1}{2}} = \tfrac{1}{2}(V^{n+1} + V^n), \qquad k = T/N$$

for sequences $\{V^n\}$. Note that, since $\chi \equiv 1$ belongs to $\mathring{S}_h^r$, (3.1) implies that

$$(U^n, 1) = (u_0^h, 1) \quad (n = 0, \ldots, N), \qquad (3.2)$$

in analogy with (2.6) for the continuous equation. Further, since ϕ is continuously differentiable, (3.1) will have a unique solution for k sufficiently small.

We observe that (3.1) is an implicit midpoint rule for the numerical integration of the ordinary differential equations resulting from the finite-element Galerkin semidiscretization in space; optimal-order error bounds for this semidiscretization method were obtained by Elliott & Zheng (1986). In the following paragraphs we analyse the convergence of the fully discrete scheme (3.1). A useful tool in the analysis is the elliptic projection $P_h : H_E^2(I) \rightarrow \mathring{S}_h^r$ defined by: for $v \in H_E^2(1)$, the function $P_h v$ is the unique solution of

$$(D^2 P_h v - D^2 v, D^2\chi) = 0 \quad \forall \chi \in \mathring{S}_h^r, \qquad (\chi, 1) = 0, \qquad (3.3a)$$

$$(P_h v, 1) = (v, 1). \qquad (3.3b)$$

The existence of a unique $P_h v$ satisfying (3.3) follows from the Lax–Milgram theorem and the Friedrichs-Poincaré inequality

$$\|\eta\|_2 \leq C(|\eta|_2 + |(\eta, 1)|) \quad \forall \eta \in H_E^2(I). \qquad (3.4)$$

It follows as in Elliott & Zheng (1985) that

$$\|P_h v - v\|_0 \leq Ch^2 \|v\|_3 \quad (r = 3), \qquad \|P_h v - v\|_0 \leq Ch^r \|v\|_r \quad (r \geq 4). \qquad (3.5a,b)$$

THEOREM 3.1 *Suppose that the solution $u(t)$ of (1.1) is sufficiently regular for a given $T > 0$ and that the solution of (3.1) satisfies*

$$\|U^n\|_\infty \leq \beta_N \quad (n = 0, \ldots, N); \qquad (3.6)$$

then

$$\|U^n - u(t_n)\|_0 \le C\Big(\|u_0^h - u_0\|_0^2 + k\sum_{j=0}^{n} \|\rho^j\|_0^2 + \int_0^T \|\rho_t(s)\|_0^2 \, ds$$

$$+ k^4 \int_0^T [\|u_{ttt}(s)\|_0^2 + \|u_{tt}(s)\|_2^2] \, ds\Big)^{\frac{1}{2}}, \quad (3.7)$$

where $t_n = nk$, $\rho^n = P_h u^n - u(t_n)$, *and* $P_h u^n \equiv P_h u(t_n)$. *The constant C depends on* γ, β_N, T, *and* $\|u(t)\|_\infty$ *for* $t \in [0, T]$.

Proof. We use the standard error decomposition:

$$U^n - u(t_n) = [U^n - P_h u^n] + [P_h u^n - u(t_n)] = \theta^n + \rho^n.$$

To obtain (3.7), we estimate θ^n. Using (3.1), we have

$$(\partial_t \theta^n, \chi) + \gamma(D^2\theta^{n+\frac{1}{2}}, D^2\chi) = (\phi(U^{n+\frac{1}{2}}) - \phi(u(t_{n+\frac{1}{2}})), D^2\chi)$$

$$- (\partial_t P_h u^n - u_t(t_{n+\frac{1}{2}}), \chi) - \gamma(D^2[\tfrac{1}{2}u(t_{n+1}) + \tfrac{1}{2}u(t_n) - u(t_{n+\frac{1}{2}})], D^2\chi).$$

Setting $\chi = \theta^{n+\frac{1}{2}}$, the above becomes

$$(\partial_t \theta^n, \theta^{n+\frac{1}{2}}) + \gamma \|\theta^{n+\frac{1}{2}}\|_2^2 \le [\|\phi(U^{n+\frac{1}{2}}) - \phi(u(t_{n+\frac{1}{2}}))\|_0 +$$

$$\|\partial_t P_h u^n - u_t(t_{n+\frac{1}{2}})\|_0 + \gamma\|\tfrac{1}{2}u(t_{n+\frac{1}{2}}) + \tfrac{1}{2}u(t_n) - u(t_{n+\frac{1}{2}})\|_2]\|\theta^{n+\frac{1}{2}}\|_2. \quad (3.8)$$

Using the Schwarz inequality, we obtain

$$(\partial_t \theta^n, \theta^{n+\frac{1}{2}}) \le C(I_1 + I_2 + I_3)^2, \quad (3.9)$$

where the I's are the three terms in the first factor on the right-hand side of (3.8).
Estimate I_3:

$$I_3 = \gamma \left\| \int_{t_{n+\frac{1}{2}}}^{t_{n+1}} (s - t_{n+\frac{1}{2}})u_{tt}(s) \, ds - \int_{t_n}^{t_{n+\frac{1}{2}}} (s - t_{n+\frac{1}{2}})u_{tt}(s) \, ds \right\|^2$$

$$\le \gamma k^{\frac{3}{2}} \Big(\int_{t_n}^{t_{n+1}} \|u_{tt}(s)\|_2^2 \, ds\Big)^{\frac{1}{2}}.$$

Estimate I_1:

$$I_1 = \|\phi'(\eta)[U^{n+\frac{1}{2}} - u(t_{n+\frac{1}{2}})]\|_0 \le C \|U^{n+\frac{1}{2}} - u(t_{n+\frac{1}{2}})\|_0,$$

where C is dependent on β_N and $\|u(t_{n+\frac{1}{2}})\|_\infty$. Then

$$I_1 \le C[\|\theta^{n+\frac{1}{2}}\|_0 + \tfrac{1}{2}(\|\rho^{n+1}\|_0 + \|\rho_n\|_0) + \|\tfrac{1}{2}u(t_{n+1}) + \tfrac{1}{2}u(t_n) - u(t_{n+\frac{1}{2}})\|_0].$$

The last term is estimated in the same way as I_3.
Finally we consider I_2.

$$I_2 \le \|\partial_t P_h u^n - \partial_t u(t_n)\|_0 + \|\partial_t u(t_n) - u_t(t_{n+\frac{1}{2}})\|_0$$

$$= k^{-1}\|\rho^{n+1} - \rho^n\|_0 + \|k^{-1}(u(t_{n+1}) - u(t_n)) - u_t(t_{n+\frac{1}{2}})\|_0$$

$$\le k^{-\frac{1}{2}}\Big(\int_{t_n}^{t_{n+1}} \|\rho_t(s)\|_0^2 \, ds\Big)^{\frac{1}{2}}$$

$$+ k^{-1}\Big(\Big\|\int_{t_{n+\frac{1}{2}}}^{t_{n+1}} (s - t_{n+\frac{1}{2}})^2 u_{tt}(s) \, ds - \int_{t_n}^{t_{n+\frac{1}{2}}} (s - t_{n+\frac{1}{2}})^2 u_{tt}(s) \, ds \Big\|_0\Big)$$

$$\le k^{-\frac{1}{2}}\Big(\int_{t_n}^{t_{n+1}} \|\rho_t(s)\|_0^2 \, ds\Big)^{\frac{1}{2}} + k^{\frac{3}{2}}\Big(\int_{t_n}^{t_{n+1}} \|u_{ttt}(s)\|_0^2 \, ds\Big)^{\frac{1}{2}}$$

With these estimates, (3.9) becomes

$$\tfrac{1}{2}k^{-1}(\|\theta^{n+1}\|_0^2 - \|\theta^n\|_0^2) \leq C(\|\theta^{n+\frac{1}{2}}\|_0^2 + w_n),$$

where

$$w_n = \|\rho^{n+1}\|_0^2 + \|\rho_n\|_0^2 + k^3\left(\int_{t_n}^{t_{n+1}} \|u_{tt}(s)\|_2^2 + \|u_{ttt}(s)\|_0^2 \, ds\right) + k^{-1}\int_{t_n}^{t_{n+1}} \|\rho_t(s)\|_0^2 \, ds,$$

which yields

$$\|\theta^{n+1}\|_0^2 \leq \frac{1+Ck}{1-Ck}\|\theta^n\|_0^2 + Ckw_n.$$

Iterating this inequality, we have

$$\|\theta^n\|_0^2 \leq C(T)\|\theta^0\|_0^2 + Ck\sum_{j=0}^{n-1} w_j.$$

Noting that

$$\|\theta^0\|_0^2 \leq \|\rho^0\|_0^2 + \|U^0 - u_0\|_0^2,$$

we obtain (3.7).

We consider the application of (3.7) to finite-element spaces. If $r = 4$, so that S_r^h consists of C^2 piecewise cubics, then

$$\|\rho^n\|_0 \leq Ch^4 \|u\|_3,$$

and thus (3.7) would become

$$\|U^n - u(t_n)\|_0 \leq C(h^8 + k^4 + \|u_0^h - u_0\|_0^2)^{\frac{1}{2}}. \tag{3.10}$$

If $r = 3$, so that S^h consists of C^1 piecewise quadratics, then

$$\|\rho^n\|_0 \leq Ch^2 \|u\|_3,$$

and thus (3.7) would become

$$\|U^n - u(t_n)\|_0 \leq C(h^4 + k^4 + \|u_0^h - u_0\|_0^2)^{\frac{1}{2}}. \tag{3.11}$$

The initial data u_0^h for the numerical scheme was obtained from u_0 by the L^2-projection P_h^0, defined by

$$(P_h^0 u - u_0, \chi) = 0 \quad \forall \chi \in S_h^r.$$

With this approximation of the initial data, (3.10) becomes an $O((h^8 + k^4)^{\frac{1}{2}})$ bound and (3.11) is $O((h^4 + k^4)^{\frac{1}{2}})$.

Remark. Although Theorem 3.1 shows that our method will converge optimally, it does not guarantee accuracy unless we make h small. Reviewing the proof, we note that C is proportional to γ^{-1}. Since γ is small, this weakens the estimate. Another loss comes from the constant's dependence on the derivatives of u. Recall that we expect u to tend to separation patterns with sharp interfaces where u will possess large derivatives in x.

The implementation of (3.1) requires the solution of a nonlinear system of equations at each time step. To solve these, a predictor–corrector method was used; the correction step was repeated until the successive iterates converged.

All the calculations were done on a VAX 780 with double-precision arithmetic. (Floating-point error is approximately $1 \cdot 0 \times 10^{-14}$). The iterations to solve the nonlinear system on each time step were judged to have converged when the difference between successive iterates was less than approximately $1 \cdot 0 \times 10^{-7}$. Stepsize was adjusted automatically by the program; generally 4–5 iterations were used on each time step.

To obtain the predicted solution W^{n+1} from U^n, we solve the following modification of (3.1):

$$k^{-1}(W^{n+1} - U^n, \chi) + \tfrac{1}{2}\gamma(D^2(W^{n+1} + U^n), D^2\chi)$$
$$+ \tfrac{1}{2}(\phi'(U^n)D(W^{n+1} + U^n), D\chi) = 0, \qquad (3.12)$$

where U^n is used to linearize. For the correction steps we find U_j^{n+1}, for $j = 1, 2, \ldots$, by the equation

$$k^{-1}(U_j^{n+1} - U^n, \chi) + \tfrac{1}{2}\gamma(D^2(U_j^{n+1} + U^n), D^2\chi)$$
$$+ \tfrac{1}{2}(\phi'(\tfrac{1}{2}U_j^{n+1} + \tfrac{1}{2}U^n)D(U_j^{n+1} + U^n), D\chi) = 0, \qquad (3.13)$$

where we set $U_0^{n+1} = W^{n+1}$. Given a basis for S_h^r, both (3.12) and (3.13) lead to
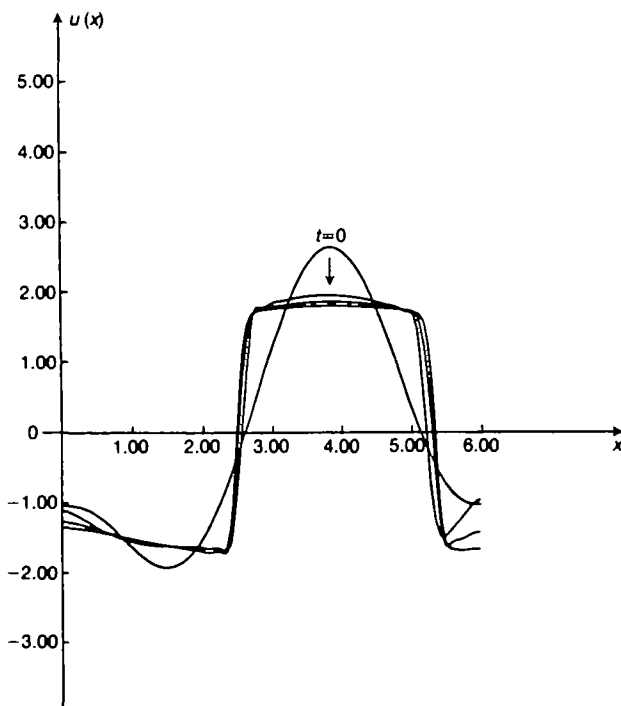
FIG. 3.1.
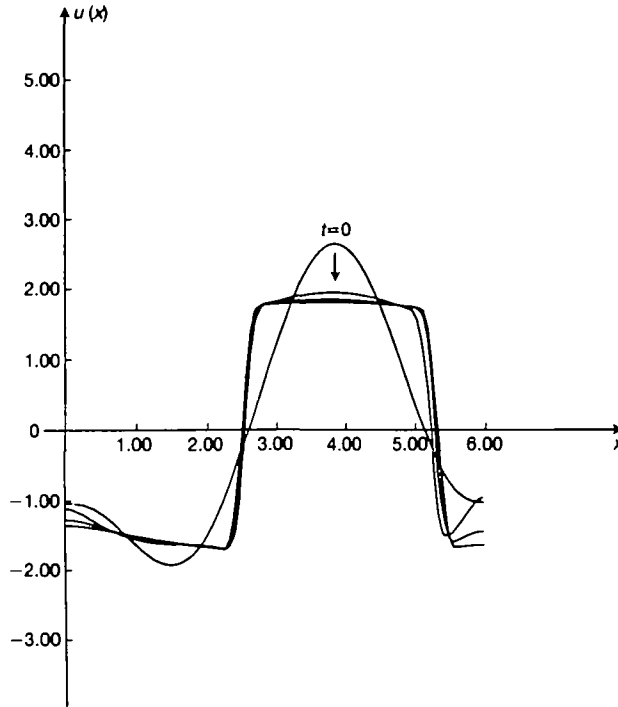
FIG. 3.2.

linear systems of equations which can be solved provided k is sufficiently small. We used B-splines as basis functions for the spaces S_h^r.

To conclude, we remark on the choice of the finite-element space S_h^r. As discussed in Section 2 when γ is small, the steady-state solution is very close to a piecewise constant function. In this situation, we expect that the spline space with the lowest degree of smoothness is preferable, and this supported by Figs 3.1 and 3.2, which show the concentration u plotted as a function of x for several times with the direction of increasing time being defined by the arrow. In both, we computed the solution of (1.1) with $\gamma = 0.005$, $L = 6.0$, and the initial data a ninth-degree polynomial with mean value $M = 0$. The same mesh, 40 nodes, and time step $\Delta t = 0.002$ were used in the computations. We used C^2 cubics in Fig. 3.1 and C^1 quadratics in Fig. 3.2. We believe the wiggles near the corners in Fig. 3.1 result from the difficulties C^2 functions have in approximating a function that is nearly piecewise constant. The quadratics in Fig. 3.2 handle this better.

4. Numerical results

In this section, we illustrate the discussion of Section 2 using the results of numerical experiments performed with the method described in Section 3. In all experiments, C^1 quadratics were used.

4.1 *Asymptotic Convergence to the Steady state $u = M$*

Choosing the free energy Ψ to be

$$\Psi(u) = \tfrac{1}{12}u^4 - \tfrac{1}{2}u^2, \tag{4.1a}$$

we find that the binodal points are

$$u_a = -\sqrt{3}, \qquad u_b = \sqrt{3}, \tag{4.1b}$$

and the spinodal points are

$$u_a^s = -1, \qquad u_b^s = 1. \tag{4.1c}$$

Because Ψ is symmetric about $u = 0$, we have the binodal points corresponding to the absolute minima of Ψ, i.e. $\Psi_m = \Psi(u_a) = \Psi(u_b)$.

We will perform computations to support statement (v) of Theorem 2.1 using the free energy Ψ and a ninth-degree polynomial

$$p(x) = x^4(x - L)^4(x - r_0) + M_0,$$

for initial data with $r_0 = 2 \cdot 2 \dots$; here, L is the interval length and M_0 is picked so that

$$\int_0^L p(x) \, dx = 0.$$

The results of two experiments are shown which exemplify conditions (C2) and (C3). We let $L = 6 \cdot 0$, and use a mesh with 240 nodes with a time step of $0 \cdot 005$ in each. The concentration u is plotted for various times and with differing parameters in Figs. 4.1 and 4.2.

Figure 4.1 displays the results when the mean value M of u_0 is sufficiently large. We expect that, when M lies in the stable region, to the right or left of the binodal values, the solution of (1.1) will tend to its mean value M. In this experiment, we took $\gamma = 0 \cdot 0005$ and

$$u_0(x) = Ap(x) + M, \tag{4.2}$$

where $M = 3 \cdot 0$ and A is picked so that

$$\|u_0 - M\|_\infty \cong 2.7. \tag{4.3}$$

The time spacing in the plots of Fig. 4.1 is roughly $0 \cdot 5$ and the last one was at $t = 2 \cdot 7$.

Figure 4.2 shows an experiment made while studying (C3) (See Remark 3). Here we took $\gamma = 0 \cdot 005$ and u_0 as in (4.2), except with $M = 1 \cdot 7$ close to the minimum of Ψ. The function u_0 does not satisfy the requirements of our theorem, because the fluctuations are too large; however, it is interesting to see that $u(\cdot, t)$ still converges to the constant function M. Plots were made at time intervals of roughly $0 \cdot 4$ till $t = 7 \cdot 6$.

4.2 *Spinodal Decomposition*

In our numerical experiments we observed that, if the initial data had mean values in the spinodal interval (u_a^s, u_b^s), then phase separation took place. The
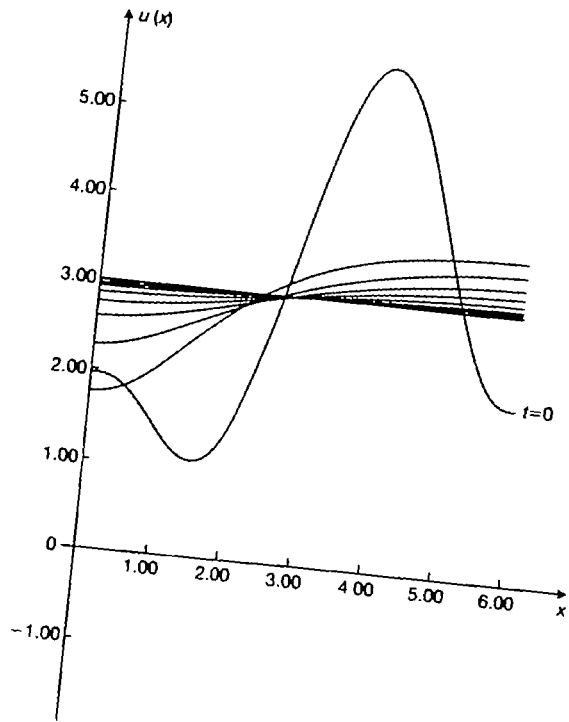
FIG. 4.1.
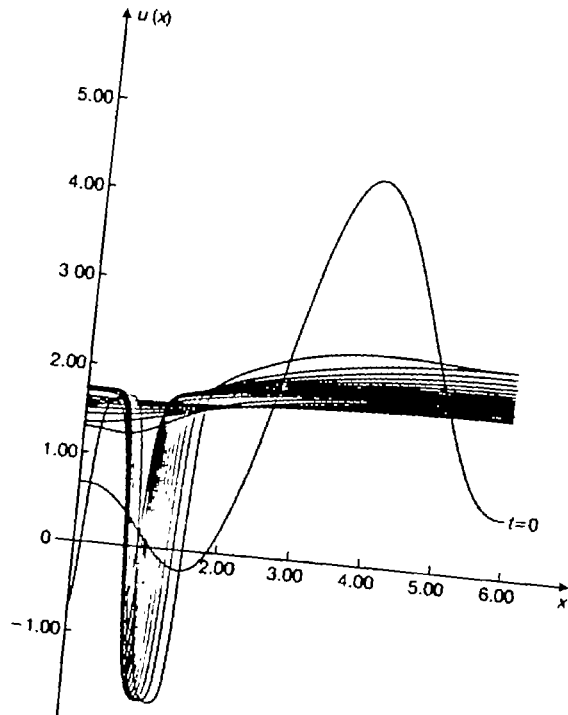
FIG. 4.2.
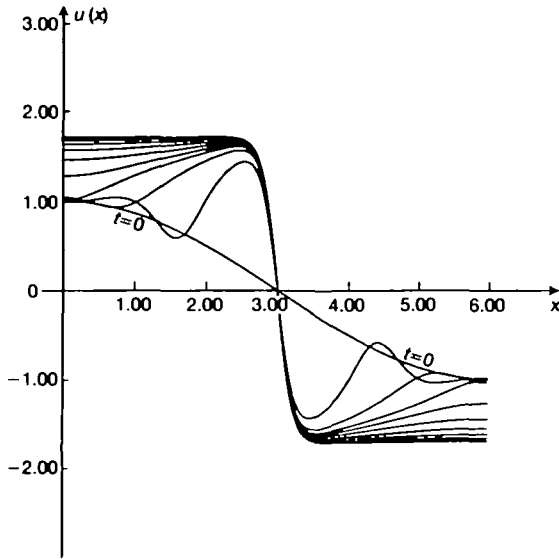
FIG. 4.3.

solutions tended to nearly piecewise constant functions exhibiting a fine-grained structure when γ is small, with grains being identified by the binodal values u_a and u_b. In all the computations of this section, we stopped the time-stepping once a pattern was reached that appeared to be stable. One can observe that, except for Fig. 4.3, all the 'stable' patterns are nonmonotone functions and are not periodic; thus they are not steady-state solutions. We therefore do not expect them to remain. In Sections 4.3 and 5 we will address these inconsistencies.

In all the experiments, C^1 quadratics were used and initial data had mean value zero. We took

$$\Psi(u) = \tfrac{1}{12}u^4 - \tfrac{1}{4}u^2,$$

with binodal values $\pm\sqrt{3}$ in each diagram, except Figs 4.5 and 4.6, where

$$\Psi(u) = \tfrac{1}{4}u^4 - \tfrac{1}{2}u^2,$$

with binodal points at ± 1.

Table 4.1 summarizes the parameters used.

TABLE 4.1

Fig.	γ	Time step (Δt)	Nodes
4.3	0·02	0·001	80
4.4	0·07	0·001	80
4.5, 4.6	0·03	0·01	120
4.7, 4.8	0·03	0·02	100
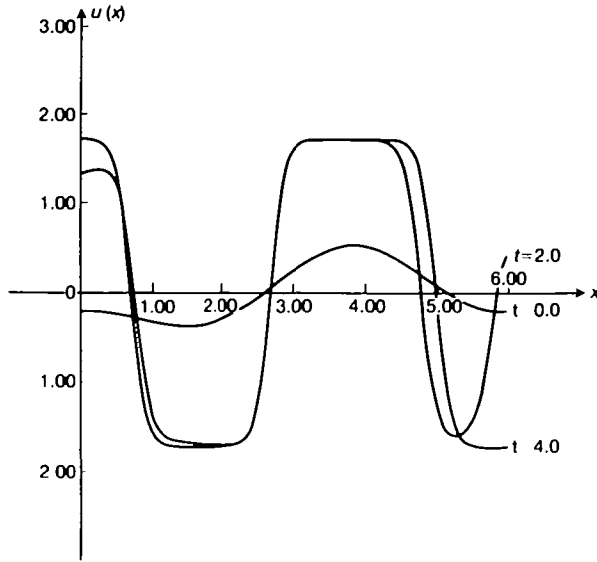
FIG. 4.4.

Figure 4.3 shows the evolution from $u_0(x) = \cos \frac{1}{6}\pi x$; Fig. 4.4 shows the evolution from the polynomial in (4.2) with A set so that $\|u_0\|_\infty \approx 0\cdot 5$. The pattern shown at $t = 4\cdot 0$ remained, except for a slight movement till $t = 60\cdot 0$.

The pairs of figures 4.5–4.6 and 4.7–4.8 show evolution from random initial data. The pattern in Fig. 4.6, which is u at $t = 72$, was obtained at $t = 8$. The pattern in Fig. 4.8, which is u at $t = 232$, was obtained at $t = 8$ also.
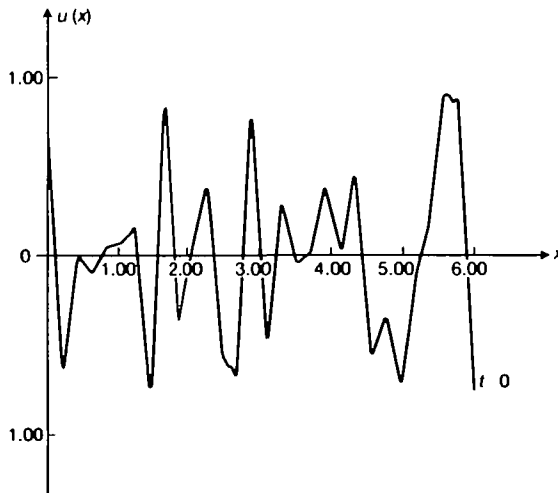
FIG. 4.5.
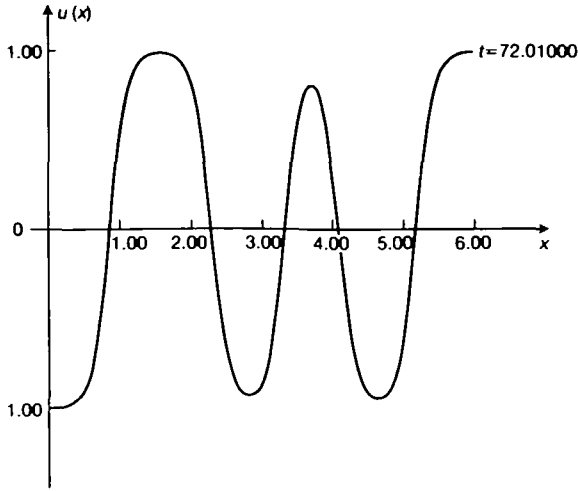
FIG. 4.6.

4.3 *Linear Combinations of Van Der Waal's* tanh *Solution*:

In numerical experiments, we observed that the solution $u(t)$ tends to, and remains at for a long time, patterns that are nearly piecewise constant (Figs 4.4, 4.6, and 4.8). Since these are generally not periodic (in the manner Carr, Gurtin, & Slemrod (1984) describe), they are not solutions of the steady-state equation, and thus we do not expect them to be stable. These patterns we classify as being metastable. In the case $\Psi(u)$ being symmetric about $u = 0$, we can obtain explicit
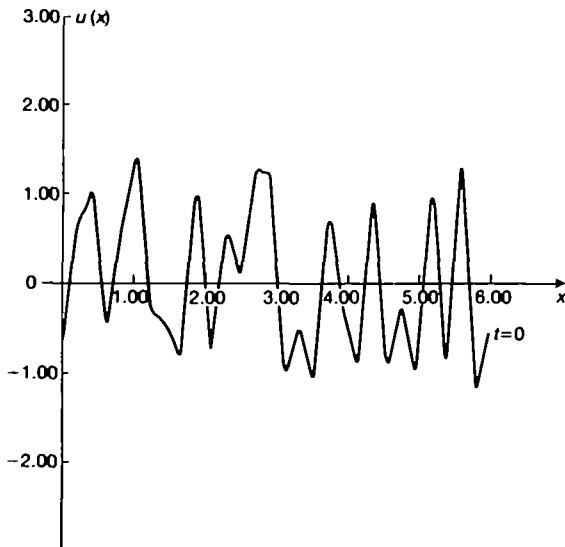
FIG. 4.7.
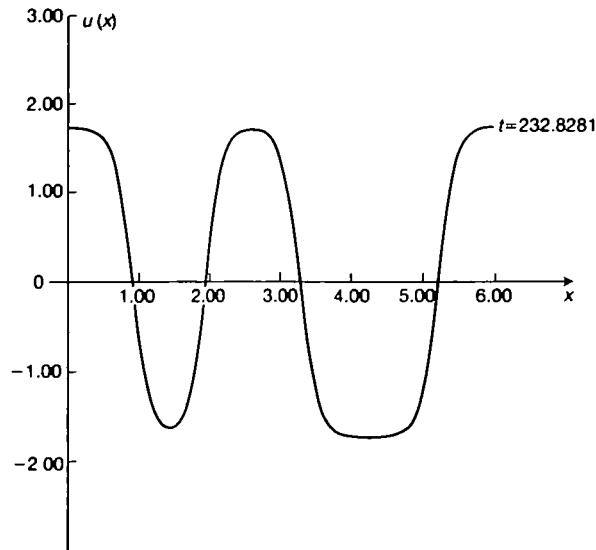
FIG. 4.8.

formulae for a class of nearly piecewise constant functions that almost satisfy the steady-state equation. Numerical experiments indicate that this class of functions exhibits metastability.

Consider the steady-state equation (2.10) with $\sigma = 0$:

$$\gamma u'' = \varphi(u), \tag{4.4}$$

where

$$\varphi(u) = \gamma_1(u - m)u(u + m), \qquad \gamma_1 > 0.$$

Van Der Waal's tanh solution (See Novick-Cohen & Segal (1984) or Langer (1971)) satisfies the equation (4.4) but not the Neumann boundary condition; however, its first derivative at the endpoints is very small, particularly if γ is small.

We shall study special linear combinations of these tanh solutions that nearly satisfy the equation (4.4). In a numerical example, we will verify that these functions are exceedingly stable. By making the transformation

$$v(z) = m^{-1}[u(\varepsilon z) + m],$$

where $\varepsilon = (\gamma/\gamma_1 m^2)^{\frac{1}{2}}$, equation (4.4) becomes

$$v'' = \bar\varphi(v) \quad (0 < z < L/\varepsilon), \tag{4.5}$$

where $\bar\varphi(v) = (v - 2)(v - 1)v$. The functions

$$1 \pm \tanh\left[2^{-\frac{1}{2}}(z - \xi)\right]$$

satisfy (4.5). For $\xi < \eta$, set

$$S_{\xi,\eta}(z) = \tanh\left[2^{-\frac{1}{2}}(z - \xi)\right] - \tanh\left[2^{-\frac{1}{2}}(z - \eta)\right].$$

We will show that

$$v(z) = \sum_{i=1}^{n-1} S_{\xi_i \eta_i}(z) + \{1 - \tanh [2^{-\frac{1}{2}}(z - \eta_0)]\} + \{1 + \tanh [2^{-\frac{1}{2}}(z - \xi_n)]\} \quad (4.6)$$

satisfies (4.5) except for a small error.

Consider

$$w'' = (w + 2)(w + 1)w. \quad (4.7)$$

If v satisfies (4.5), then $w = v - 2$ satisfies (4.7). Note that

$$\lambda_\xi(z) = \tanh [2^{-\frac{1}{2}}(z - \xi)] - 1, \qquad \lambda_\eta(z) = -\tanh [2^{-\frac{1}{2}}(z - \eta)] - 1$$

are solutions of (4.7), and the product $\lambda_\xi \lambda_\eta$ is small as long as $\xi < \eta$. A short calculation shows that, if $w(z) = \lambda_\xi(z) + \lambda_\eta(z)$, where $\xi < \eta$, then

$$w'' = (w + 1)(w + 2)w + \bar{E}(z),$$

with $|\bar{E}(z)| \leq 8 |\lambda_\xi(z)\lambda_\eta(z)|$. Transforming back to (4.5), we have

$$s''_{\xi\eta} = \tilde{\varphi}(s_{\xi\eta}) + \bar{E}(z).$$

If $v(z)$ is given by (4.6), we can show that

$$v'' = \tilde{\varphi}(v) + E(z),$$

where

$$|\bar{E}(z)| \leq 8n |\lambda_\alpha(z)\lambda_\beta(z)|, \qquad \beta - \alpha = \min_{i,j} |\xi_i - \eta_j|.$$

Transforming these results to equation (4.4) we have that

$$u(x) = \sum_{i=1}^{n-1} [T_{a_i}(x) - T_{b_i}(x)] + [m - T_{b_0}(x)] + [T_{a_n}(x) + m] - m$$

satisfies

$$\gamma u'' = \varphi(u) + \delta,$$

where $|\delta(x)| \leq 8n\gamma_1 |[T_p(x) - m][T_q(x) - m]|$, with

$$q - p = \min_{i,j} |b_i - a_j|, \qquad a_i = \xi_i/\varepsilon, \qquad b_i = \eta_i/\varepsilon,$$

$$T_\sigma(x) = m \tanh [m(\tfrac{1}{2}\gamma_1/\gamma)^{\frac{1}{2}}(x - \sigma)].$$

EXAMPLE. Let $\varphi(u) = \tfrac{1}{3}u^3 - u$ so $m = \sqrt{3}$ and let

$$u(x) = (\sqrt{3} - T_{L/6}) + (T_{L/3} - T_{2L/3}) - \sqrt{3}$$

$$= -T_{L/6} + (T_{L/3} - T_{2L/3}).$$

For δ we have the bound

$$|\delta(x)| \leq 16 |\{\tanh [(2\gamma)^{-\frac{1}{2}}(x - \tfrac{1}{6}L)] - 1\}\{\tanh [(2\gamma)^{-\frac{1}{2}}(x - \tfrac{1}{6}l)] - 1\}|.$$

Take $L = 6$ and consider the bounds for δ for several γ at $x = 1\cdot5$:

$$|\delta(1\cdot5)| \leq 16 \,|\tanh\,[(2\gamma)^{-\frac{1}{2}}(0\cdot5)] - 1|^2.$$

TABLE 4.2

γ	Bound for $\delta(1.5)$
0·05	0·10
0·02	3×10^{-3}
0·005	$1\cdot3 \times 10^{-7}$

To verify that these approximate solutions are candidates for a class of metastable patterns, we ran several numerical experiments where the initial data $u_0(x)$ was set as a linear combination of tanh solutions.

Figure 4.9 shows the plots for $u(t)$ at $t = 0, 5, 10, \ldots, 60$, where

$$u_0(x) = -T_1(x) + T_2(x) - T_4(x) - \sqrt{3}, \qquad \varphi(u) = \tfrac{1}{3}u^3 - u, \qquad L = 6, \qquad \gamma = 0\cdot02.$$

A mesh with 120 nodes was used, and a time step of 0·01. Except for a slight movement along the interfaces, $u(t)$ has remained on the given tanh solution.

In Figs 4.10–4.14 we show the long time evolution of u. We had parameters

$$u_0(x) = -T_{2\cdot5}(x) + T_{5\cdot5}(x) - \sqrt{3}, \qquad \varphi(u) = \tfrac{1}{3}u^3 - u, \qquad L = 6, \qquad \gamma = 0\cdot03.$$

A mesh with 100 nodes was used and time step 0·02. The plots shown are $u(t)$ at $t = 0, 28, 124, 148, 160$.

Note that $u(t)$ has hardly changed from $t = 0$ to $t = 28$ and, except for the
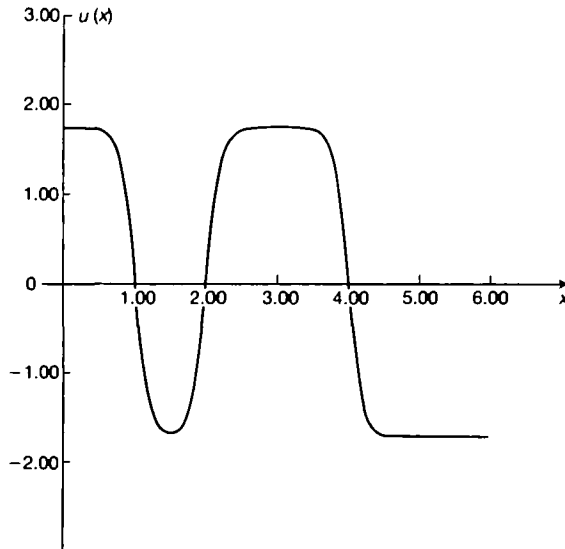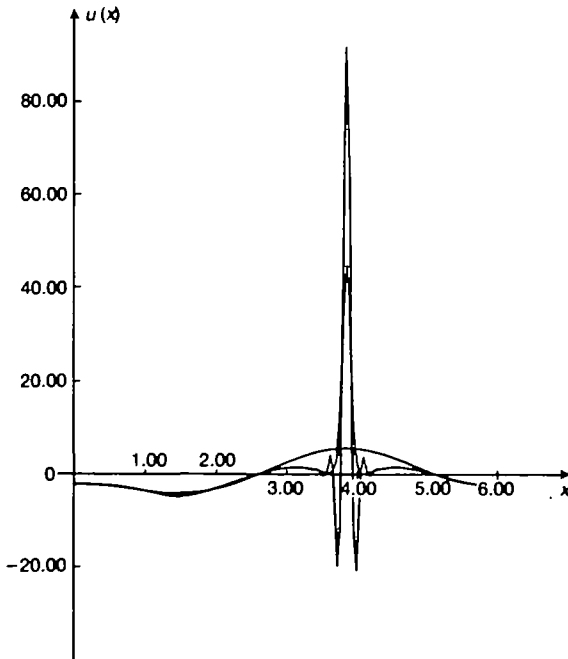

FIG. 4.9.
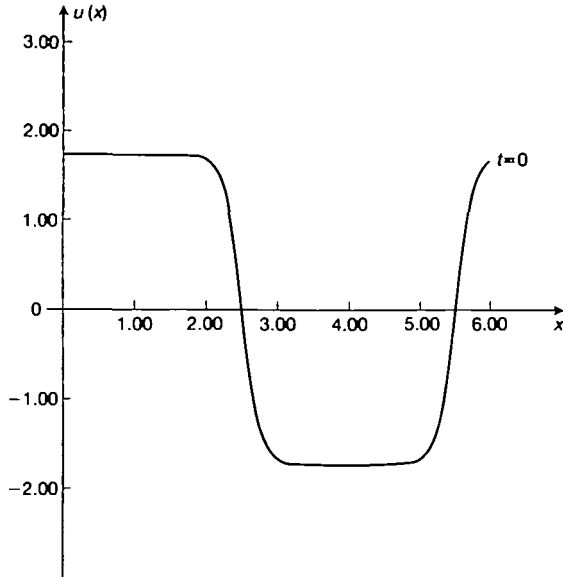
FIG. 4.10.
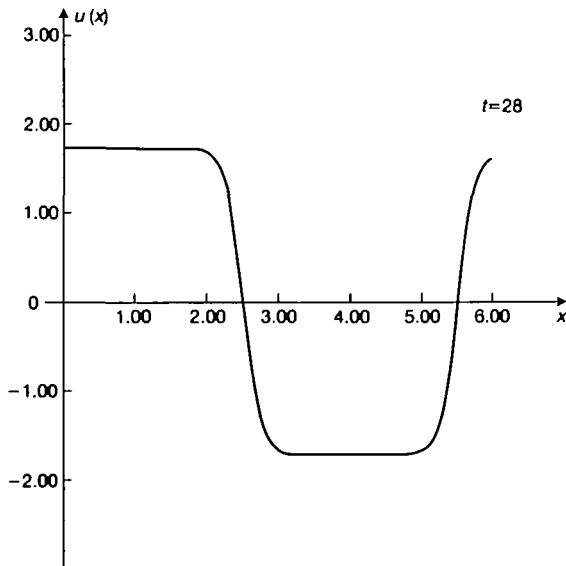
FIG. 4.11.
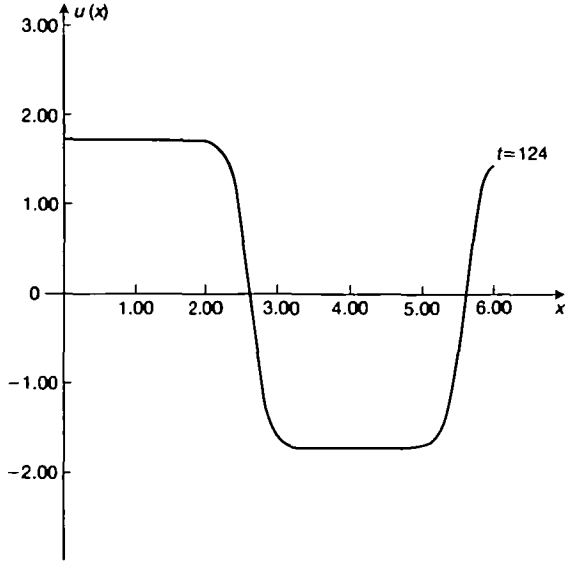
FIG. 4.12.
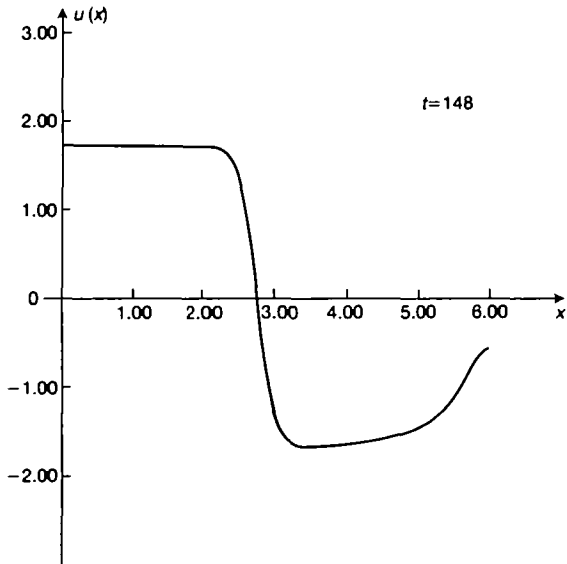
FIG. 4.13.
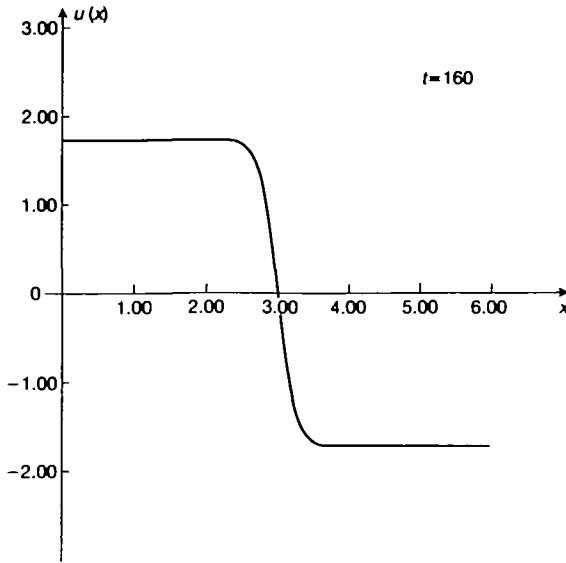
FIG. 4.14.

FIG. 4.15.

interface at $x \cong 5 \cdot 5$ falling a small amount, it is remarkably unchanged at $t = 124$. The final graphs show the transition to the monotone solution.

4.4   Finite-Time Blow-up

It was shown in Elliott and Zheng (1986) that, if $\gamma_2 < 0$ and the initial data is sufficiently large, then the solution of (1.1) will blow up in finite time. The numerical solution also exhibited this behaviour.

We studied the case when $\gamma_2 = -0 \cdot 2$, $\gamma_1 = 0$, $\gamma_0 = 1$, $\gamma = 0 \cdot 5$ and

$$u_0(x) = Ap(x).$$

where A was picked so that $\|u_0\|_\infty \cong 5 \cdot 5$, which was large enough for the numerical solution to blow up. Figure 4.12 is a good representative of the shape of the numerical solution in this example, although, in the computations when we varied the mesh refinement and time step size, we obtained blow-up times and plots which were slightly different.

This, of course, is not unusual for a blow-up calculation.

5. Future directions

In the numerical experiments exhibiting phase separation, for initial data with mean composition in the spinodal interval, we observed two characteristic processes. First there is a comparatively rapid transformation of the initial data to a fine-grained, usually nonperiodic, structure. See Figs 4.4, 4.6, 4.8, and 4.9. These structures are metastable in the sense that they persist for a long time without apparent change. This transformation is evidently spinodal decomposition. The second process is a very slow transformation to a coarse-grained structure monotone in x. See Figs 4.11–4.13. In this process, akin to nucleation, the composition of a grain is unchanged but the width slowly increases.

An interesting mathematical problem related to metastability is the following: Identify metastable configurations, and obtain estimates on the length of time that u remains in a neighbourhood of a particular metastable solution. Weinberger (1985) proved theorems of this type for a parabolic system of equations.

We performed several long-time computations where u_0 had a random structure. In all of the calculations, $u(t)$ did not reach the monotone solution in a time scale on which we could compute. These calculations generally took a long time on the VAX and thus we were limited in how far we could refine our mesh and time step. Figures 5.1–5.12 show a sample computation.

In this experiment, $\Psi(u) = \frac{1}{12}u^4 - \frac{1}{2}u^2$, $\gamma = 0 \cdot 03$, $L = 6 \cdot 0$, the mesh had 100 nodes and the time step was $0 \cdot 02$. We computed the free energy on each time step and found it decreased as expected: see Table 5.1.

It is interesting to consider u_t. Figures 5.8–5.12 display u_t computed by the formula

$$u_t \doteq (U^n - U^{n-1})/\Delta t$$

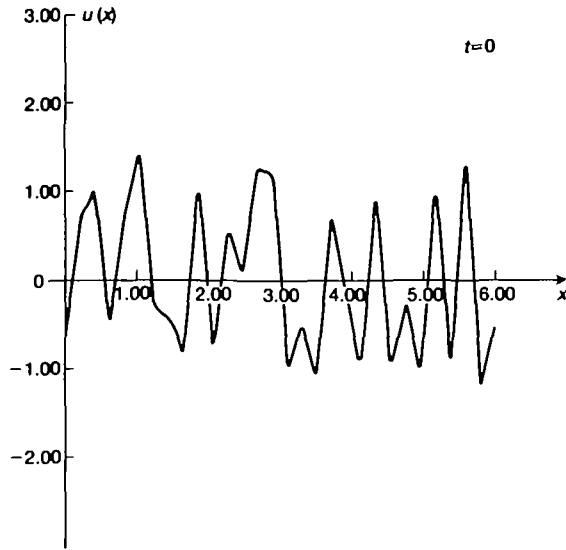where $U^n \approx u(\cdot, n\Delta t)$. In Table 5.2 we note the maximum value of u_t.

FIG. 5.1.

We decided to stop the calculation at $t = 600$, because neither u nor u_t had changed from $t = 404$ to $t = 596$.

This last computation suggests the following numerical-analysis questions: What is the long-time accuracy of the numerical method? Does the approximate problem have the same stability properties as the continuous problem?
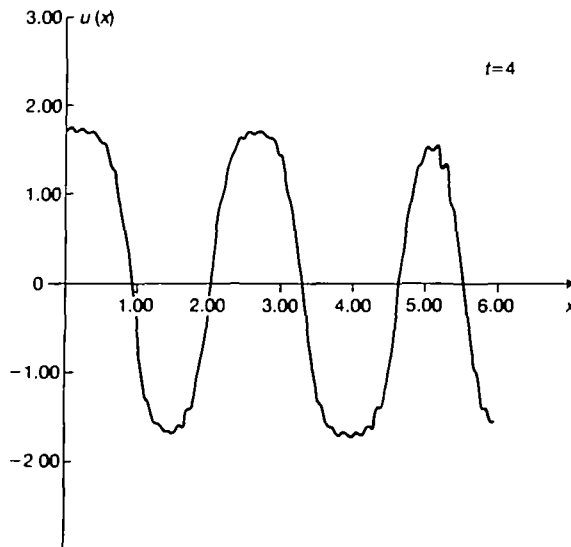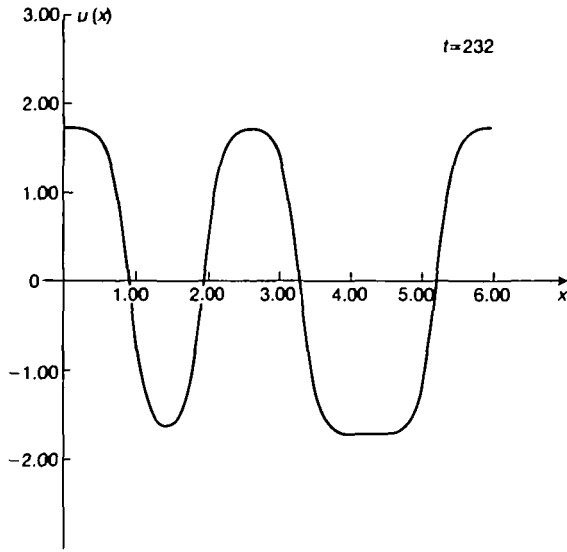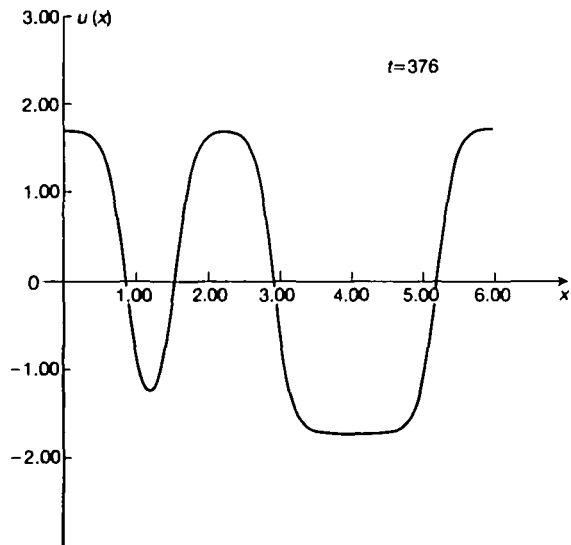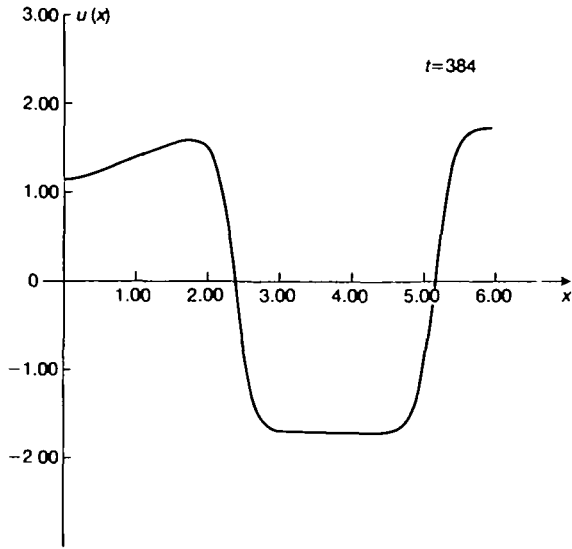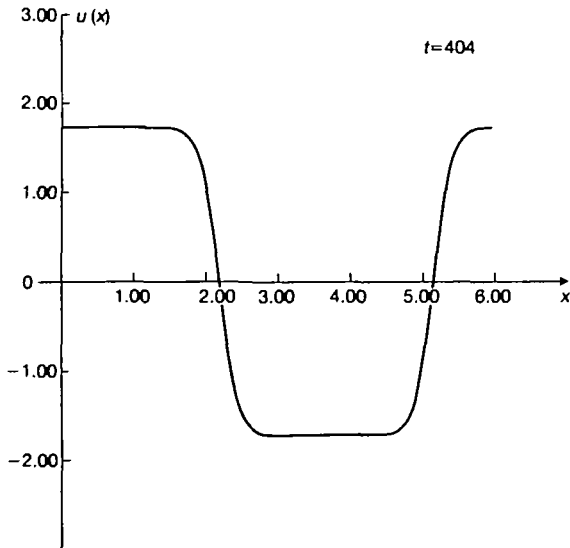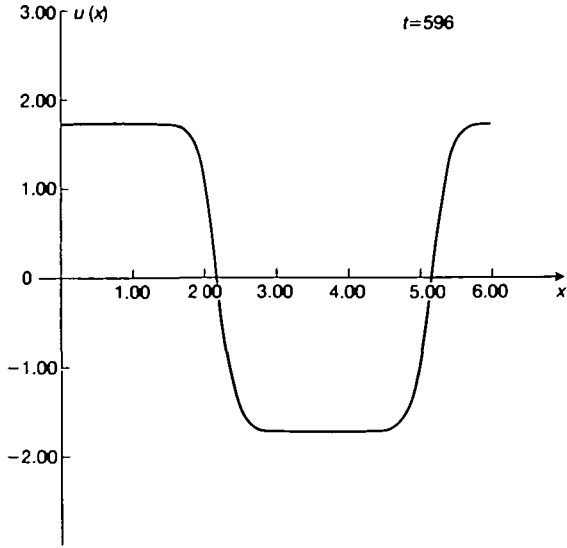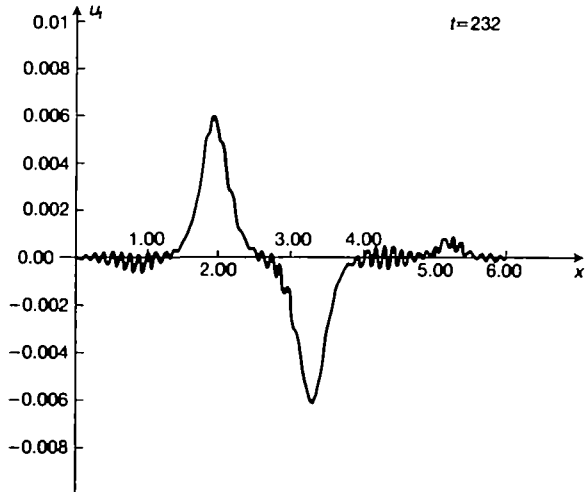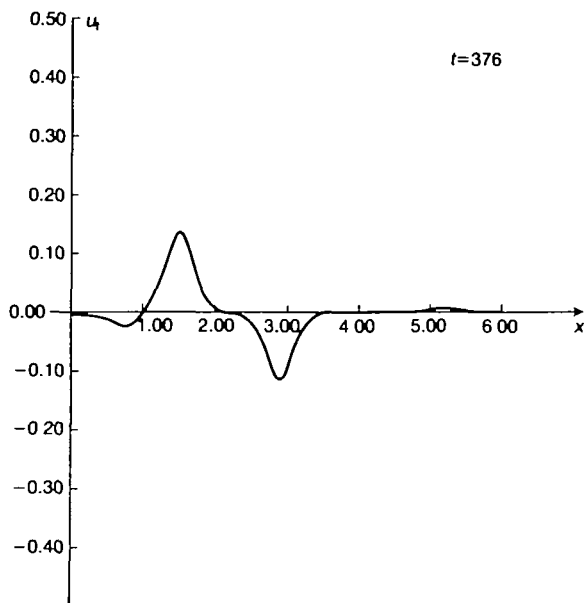
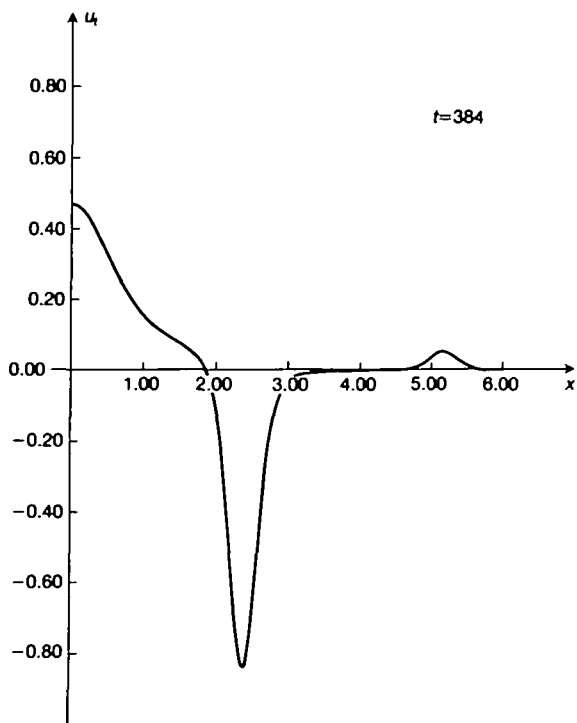

FIG. 5.2.

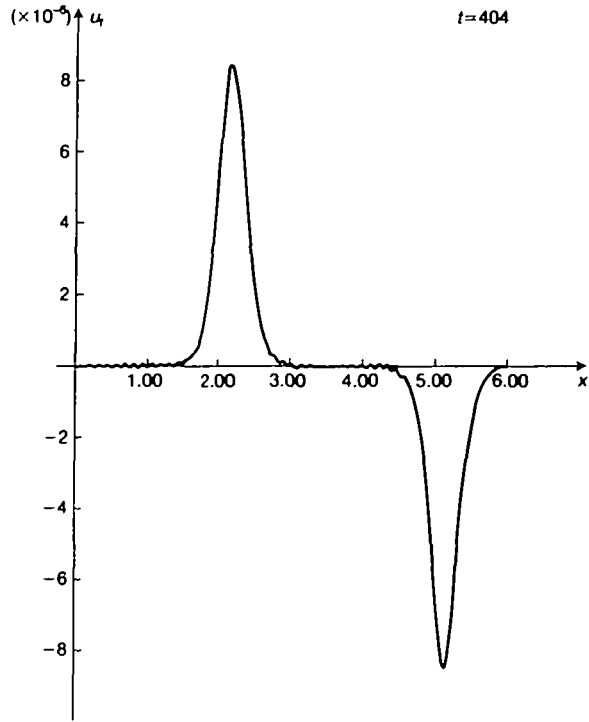FIG. 5.3.

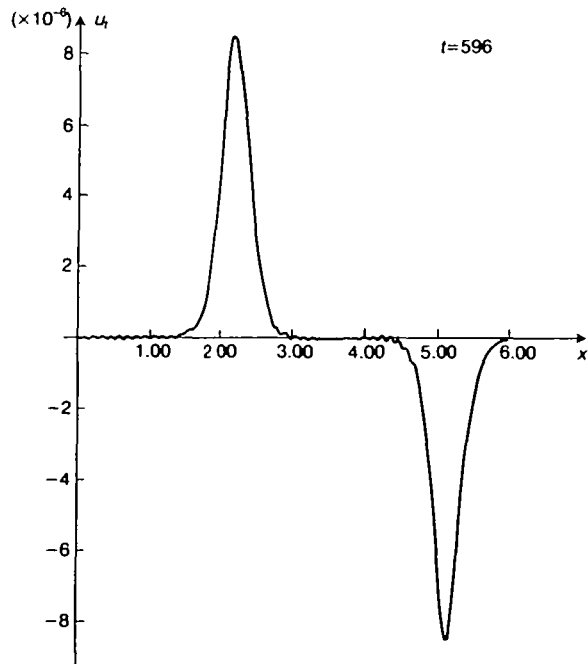FIG. 5.4.

FIG. 5.5.

FIG. 5.6.

FIG. 5.7.

FIG. 5.8.

FIG. 5.9.

FIG. 5.10.

Fig. 5.11.

Fig. 5.12.

TABLE 5.1

Fig.	Time	$\mathscr{F}(u)$
5·1	0	3·02
5·2	4	−1·85
5·3	232	−2·54
5·4	376	−2·56
5·5	384	−3·31
5·6	404	−3·52
5·7	596	−3·52

TABLE 5.2

Fig.	$\|u_t\|_\infty$
5·8	0·0062
5·9	0·135
5·10	0·844
5·11	$8·5 \times 10^{-6}$
5·12	$8·5 \times 10^{-6}$

Acknowledgements

REFERENCES

CAHN, J. W. 1961 On spinodal decomposition. *Acta Metallurgica* **9**, 795–801.
CAHN, J. W. 1962 On spinodal decomposition in cubic crystals. *Acta Metallurgica* **10**, 179–183.
CAHN, J. W. & HILLIARD, J. E. 1958 Free energy of a non-uniform system. I. Interfacial free energy. *J. Chem. Phys.* **28**, 258–267.
CARR, J., GURTIN, M. E., & SLEMROD, M. 1984 Structured phase transitions on a finite interval. *Arch. rat. Mech. Anal.* **86**, 317–351.
COHEN, D. S., & MURRAY, J. D. 1981 A generalized diffusion model for growth and dispersal in a population. *J. Math Biology* **12**, 237–249.
ELLIOTT, C. M. 1985 A Stefan problem with a non-monotone constitutive relation. *IMA J. appl. Math.* **35**, 257–264.
ELLIOTT, C. M., & ZHENG SONGMU 1986 On the Cahn–Hilliard equation. *Arch. rat. Mech. Anal.* **96**, 339–357.
GUNTON, J. D., SAN-MIGUEL, M., & SAHNI, P. S. 1983 In: *Phase Transitions and Critical Phenomena* (Domb, C., & Lebowitz, J. L., Eds). Academic Press. pp. 267.
GURTIN, M. E. 1986. On phase transitions with bulk, interfacial and boundary energy. *Arch. Rat. Mech. Anal* **96**, 243–264.

HAZEWINKEL, M., KAASSHOEK, J. F., & LEYNSE, B. 1985 Pattern formation for a one dimensional evolution equation based on Thom's river basin model. Econometric Institute, Erasmus University *Report* # 8519/B.

KOCH, S. W. 1984 *Dynamics of First Order Phase Transitions in Equilibrium and Non-equilibrium Systems*. Lecture notes in Physics. Springer Verlag.

LANGER, J. S. 1971 Theory of spinodal decomposition in alloys. *Ann Physics* **65**, 53–86.

MODICA, L. 1986 Gradient theory of phase transitions with boundary contact energy (Preprint). SFB Bonn.

MODICA, L. 1987 Gradient theory of phase transitions and minimal interface criterion. *Arch. Rat. Mech. Anal.* **98**, 123–142.

NOVICK-COHEN, A., & SEGEL, L. A. 1984 Nonlinear aspects of the Cahn-Hilliard equation. *Physica* (D) **10**, 277–298.

WEINBERGER, H. 1985 On metastable patterns in parabolic systems. *IMA preprint* #164. University of Minnesota.

ZHENG SONGMU 1986 Asymptotic behaviour of the solution to the Cahn–Hilliard equation. Technical Report Series, Center for Applied Mathematics, Purdue University #25 (1986). To appear in *Applicable Analysis*.